

## Article

# High-Efficiency Stepped Separation and Recoveries of Vanadium and Molybdenum via Low-Temperature Carbonation Conversion of High-Chromium Vanadium Residue

Jiahao Zhang <sup>1,2,3,4</sup>, Nannan Xue <sup>1,2,3,4,\*</sup>, Yimin Zhang <sup>1,2,3,4,\*</sup> and Qiushi Zheng <sup>1,2,3,4</sup>

<sup>1</sup> School of Resource and Environmental Engineering, Wuhan University of Science and Technology, Wuhan 430081, China

<sup>2</sup> State Environmental Protection Key Laboratory of Mineral Metallurgical Resources Utilization and Pollution Control, Wuhan University of Science and Technology, Wuhan 430081, China

<sup>3</sup> Collaborative Innovation Center of Strategic Vanadium Resources Utilization, Wuhan University of Science and Technology, Wuhan 430081, China

<sup>4</sup> Hubei Provincial Engineering Technology Research Center of High Efficient Cleaning Utilization for Shale Vanadium Resource, Wuhan University of Science and Technology, Wuhan 430081, China

\* Correspondence: xuenannan@wust.edu.cn (N.X.); zhangyimin@wust.edu.cn (Y.Z.)

**Abstract:** High-chromium vanadium residue (HCVR (HCVR: high-chromium vanadium residue)) is an important secondary resource of valuable metals such as vanadium (V), chromium (Cr), and molybdenum (Mo). The mainstream technology for the utilization of HCVR, the Na<sub>2</sub>CO<sub>3</sub>-assisted-roasting–water-leaching method, usually requires roasting temperatures of more than 800 °C and results in the synchronous leaching of Cr with V and Mo. This makes the subsequent separation of V, Mo, and Cr in the aqueous system difficult. In this study, an efficient and clean process for the selective separation of Cr and stepped recoveries of V and Mo from HCVR is proposed via K<sub>2</sub>CO<sub>3</sub>-mediated carbonation conversion. Using this process, the roasting temperature can be reduced from more than 800 °C to 200 °C, and 83.14%, 99.94%, and 0.33% of V, Mo, and Cr, respectively, can be leached. Further, using the weakly alkaline ammonium-salt and sulfide precipitation methods, 98.28% pure V<sub>2</sub>O<sub>5</sub> and 98.65% pure MoS<sub>2</sub> can be obtained and the recoveries of V and Mo can reach 82.47% and 98.88%, respectively. While almost all Mo can be recovered from the HCVR, Cr and some V might be present as a stable ferrochrome spinel in the tailing, which may be returned to the main process for the extraction of V and Cr from vanadium slag. Thus, K<sub>2</sub>CO<sub>3</sub> might be a more effective alternative to Na<sub>2</sub>CO<sub>3</sub> for the separation and recovery of V and Mo from HCVR and, hence, may enable its more efficient utilization.

**Keywords:** carbonation conversion; stepped separation; metal recovery; waste residue utilization

**Citation:** Zhang, J.; Xue, N.; Zhang, Y.; Zheng, Q. High-Efficiency Stepped Separation and Recoveries of Vanadium and Molybdenum via Low-Temperature Carbonation Conversion of High-Chromium Vanadium Residue. *Processes* **2023**, *11*, 470. <https://doi.org/10.3390/pr11020470>

Received: 13 January 2023

Revised: 27 January 2023

Accepted: 31 January 2023

Published: 3 February 2023



**Copyright:** © 2023 by the authors. Licensee MDPI, Basel, Switzerland. This article is an open access article distributed under the terms and conditions of the Creative Commons Attribution (CC BY) license (<https://creativecommons.org/licenses/by/4.0/>).

## 1. Introduction

As an important strategic metal, vanadium can significantly improve the strength, corrosion resistance, toughness, and high-temperature resistance of steel; therefore, it is widely used in metallurgy, aerospace, chemical engineering, energy storage, and other industrial fields [1–6]. Owing to the continuous consumption of vanadium and molybdenum mineral resources, the recovery of vanadium and molybdenum from secondary resources is becoming increasingly important [7,8]. High-chromium vanadium residue (HCVR) is an important secondary resource which mainly originates from extraction processes employing vanadium slag, which contains valuable metals such as vanadium (V), chromium (Cr), and molybdenum (Mo). In China, the annual production of HCVR is

more than 500,000 tons [9]. Therefore, the valuable elements in HCVR must be recycled for an abundant supply of V and Mo.

At present, there are many methods for recovering valuable metals from HCVR, such as direct acid leaching and salt-roasting leaching [10–13]. Acid leaching [14,15] synchronously releases V and Cr from HCVR, as well as other metal impurities such as Fe and Ca, which enter the liquid phase [16] and are difficult to separate in an acidic solution. Salt roasting is often combined with water or alkali leaching, and such a process, sodium carbonate ( $\text{Na}_2\text{CO}_3$ ) roasting, is widely used to treat HCVR. Therein, stable V and Cr phases in HCVR are converted to water-soluble sodium vanadate and chromate via a reaction with  $\text{Na}_2\text{CO}_3$  at more than 800 °C [17–20]. The simultaneous release of  $\text{Cr}^{6+}$  and  $\text{V}^{5+}$  via water leaching necessitates a complex and potentially risky separation process [21,22], owing to their similar properties and  $\text{Cr}^{6+}$  reduction. Therefore, V must be selectively released from HCVR.

Recent studies have reported selective extraction of metals via the addition of potassium in the roasting process. Liu et al. [23] selectively separated and recovered lithium and cobalt from waste lithium-ion batteries via roasting using  $\text{K}_2\text{S}_2\text{O}_7$ . Ye et al. [24] selectively separated tungsten and rhenium and recovered rhenium from tungsten–rhenium wires using an alkali fused with a  $\text{KOH-K}_2\text{CO}_3$  binary molten salt.  $\text{K}_2\text{CO}_3$  may promote the carbonation conversion of HCVR to water-soluble potassium vanadate. Therefore,  $\text{K}_2\text{CO}_3$  may replace  $\text{Na}_2\text{CO}_3$  in the assisted carbonation conversion of HCVR for the selective extraction and recovery of V. Li et al. [25] discovered that the ferrochrome spinel in HCVR decomposes into a water-soluble sodium chromate at roasting temperatures above 500 °C, indicating that the roasting temperature must be below 500 °C to separate the V and Cr in HCVR.

Therefore, a new process must be developed based on low-temperature roasting to separate Cr from HCVR and, subsequently, separate and recover V and Mo. This study investigates a stepped whole process for the selective separation and high-efficiency recovery of V and Mo via the  $\text{K}_2\text{CO}_3$ -mediated low-temperature carbonation conversion of HCVR. This process has low energy consumption and can effectively separate and recover vanadium and molybdenum, which may provide technical guidance for the utilization of HCVR.

## 2. Materials and Methods

### 2.1. Materials

The HCVR used in this study originated from Panzhihua, Sichuan, China. The chemical composition of HCVR was determined by an X-ray fluorescence spectrometer (XRF), and the results are shown in Table 1. The phase composition of HCVR was determined by X-ray diffraction (XRD). The scanning angle is 5–70° and the scanning speed is 5 °/min. The results are shown in Figure 1. The main phases in the HCVR were  $\text{CaSO}_4$ ,  $\text{CaV}_2\text{O}_6$ , spinel  $\text{Cr}_{1.3}\text{Fe}_{0.7}\text{O}_3$ ,  $\text{CaMoO}_4$ ,  $\text{SiO}_2$ , and  $\text{CaCO}_3$ .  $\text{K}_2\text{CO}_3$  and  $\text{Na}_2\text{CO}_3$  were used as additives to convert  $\text{CaV}_2\text{O}_6$  and  $\text{CaMoO}_4$  to soluble vanadate and molybdate.

**Table 1.** Chemical compositions of the HCVR used in this study (wt.%).

<b>Compositions</b>	<b><math>\text{V}_2\text{O}_5</math></b>	<b>CaO</b>	<b><math>\text{Cr}_2\text{O}_3</math></b>	<b><math>\text{SiO}_2</math></b>	<b><math>\text{SO}_3</math></b>
<b>Content</b>	31.23	16.39	15.13	8.16	6.66
<b>Compositions</b>	<b><math>\text{Fe}_2\text{O}_3</math></b>	<b><math>\text{MoO}_3</math></b>	<b>Na<sub>2</sub>O</b>	<b><math>\text{Al}_2\text{O}_3</math></b>	<b>MgO</b>
<b>Content</b>	5.76	4.74	1.96	0.89	0.59

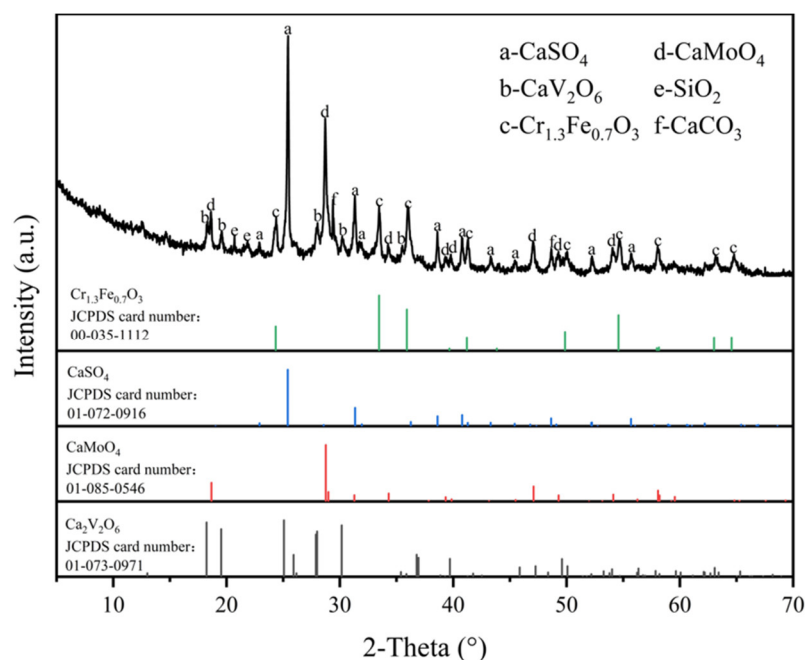


**Figure 1.** X-ray diffraction (XRD) patterns of HCVR.

## 2.2. Methods

### 2.2.1. Phase Transition and Release of Vanadium and Molybdenum

A total of 10 g HCVR was mixed with carbonate ( $\text{Na}_2\text{CO}_3$  or  $\text{K}_2\text{CO}_3$ ) in a certain proportion, placed in a muffled furnace (SX2-10-1 $\delta$  Wuhan Dianlu Experimental Electric Furnace Factory), heated from 20 °C to a certain temperature at the heating rate of 10 °C/min, and maintained there for a certain time. The carbonated HCVR (CHCVR) was used for water leaching and characterization.

During water leaching, deionized water was added to the CHCVR according to a liquid-to-solid (L/S) ratio of 2 mL/g; the stirring speed was maintained at 300 rpm, and the mixture was maintained at a certain temperature for a certain time. After leaching, the tailings and leaching liquid were separated via filtration. The leaching rates of V, Mo, and Cr were calculated using Equation (1), which represents the percentages of V, Mo, and Cr leached from the HCVR. The results were obtained from the average of three parallel experiments.

$$E = \frac{cv}{mw} \times 100\% \quad (1)$$

Here,  $E$ ,  $c$ , and  $v$  represent the leaching rate of V, Mo, or Cr; concentration of V, Mo, or Cr in the leaching liquid (g/L); and volume of the leaching liquid (L), respectively;  $m$  and  $w$  represent the HCVR mass (g) and percent mass of V, Mo, or Cr in the HCVR, respectively.

### 2.2.2. Selective Separation and Recoveries of Vanadium and Molybdenum

A certain amount of  $\text{NH}_4\text{Cl}$  was added to the leaching liquid, which was then stirred at 350 rpm for a certain time to precipitate the vanadate. After the reaction, the vanadate precipitate and Mo-supernatant were separated via filtration. The vanadate precipitation rate was calculated using Equation (2), which represents the vanadium in the vanadate precipitate as a percentage of the vanadium in the leaching liquid.

$$\eta = \left(1 - \frac{c_o v_o}{c_l v_l}\right) \times 100\% \quad (2)$$

Here,  $\eta$  represents the precipitation rate of the vanadate;  $c_o$  and  $c_l$  represent the vanadium concentrations in the Mo-supernatant and leaching liquid, respectively (g/L).  $v_o$  and  $v_l$  represent the volumes of the Mo-supernatant and leaching liquid, respectively (L).

The vanadate precipitate was calcined at 550 °C for 2 h to obtain  $V_2O_5$ .

A certain amount of  $Na_2S$  was added to the Mo-supernatant, followed by the addition of  $H_2SO_4$  to adjust the pH to a certain value. The mixture was then stirred at 350 rpm and allowed to react for a certain time at 200 °C to precipitate molybdenum. After precipitation, the wastewater and molybdenum disulfide precipitate were separated via filtration. The molybdenum disulfide precipitate was washed repeatedly with deionized water. The wastewater was returned to the water-leaching stage as washing water and a leaching medium. The precipitation rate of molybdenum was calculated using Equation (3), which represents the amount of molybdenum precipitated from the Mo-containing solution.

$$\varphi = \left(1 - \frac{m_w}{m_c}\right) \times 100\% \quad (3)$$

Here,  $\varphi$  represents the precipitation rate of molybdenum;  $m_w$  and  $m_c$  represent the masses of Mo in the wastewater and Mo-containing solution, respectively.

Figure 2 is a flow chart of the process.

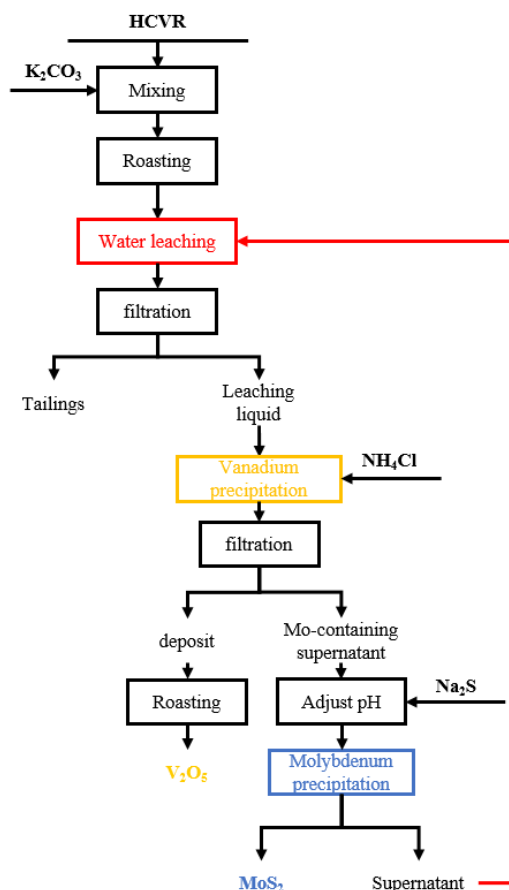


Figure 2. Flow chart of the comprehensive utilization of HCVR.

### 2.3. Characterization

Ferrous ammonium sulfate titration was used to determine the vanadium content in the vanadium-containing solution. The contents of molybdenum and chromium in the liquid were determined via inductively coupled plasma–optical emission spectrometry (ICP-OES 730, Agilent Co., Ltd, Shanghai, China.). The mineralogical composition of the sample was determined via X-ray diffraction (XRD, SmartLab SE, Rigaku Co., Ltd, Tokyo,

Japan.). The micro-morphologies and elemental distributions of the samples were determined via scanning electron microscopy (SEM, JSM-IT300, JEOL Co., Ltd, Tokyo, Japan.) and energy dispersive spectroscopy (EDS). Molybdenum sulfide products were characterized via Raman spectroscopy (LabRam HR Evolution, HORIBA (China) Trading Co., Ltd, Shanghai, China.). The thermal and mass changes accompanying the carbonation conversion of HCVR were determined via thermogravimetric analysis (TGA, DSC3+, Mettler Toledo, Ltd, Shanghai, China.). The pH of the solution is measured by a pH meter (PHS-3C Changchun Proactinium Technology Co., Ltd, Changchun, China.).

### 3. Results and Discussion

#### 3.1. Phase Transformation of Vanadium and Molybdenum and Separation of Chromium

##### 3.1.1. Effect of Temperature

To explore the different conversion effects of  $\text{Na}_2\text{CO}_3$  and  $\text{K}_2\text{CO}_3$  on vanadium and molybdenum in HCVR at different temperatures, temperature single-factor experiments were conducted and the experimental conditions were as follows: carbonation time, 120 min; molar ratio of  $\text{K}_2\text{CO}_3$  and  $\text{Ca}^{2+}$  in HCVR ( $n(\text{K}_2\text{CO}_3)/n(\text{Ca}^{2+})$ ), 1.5; leaching temperature, 80 °C; and leaching time, 100 min. Figure 3 shows the results.

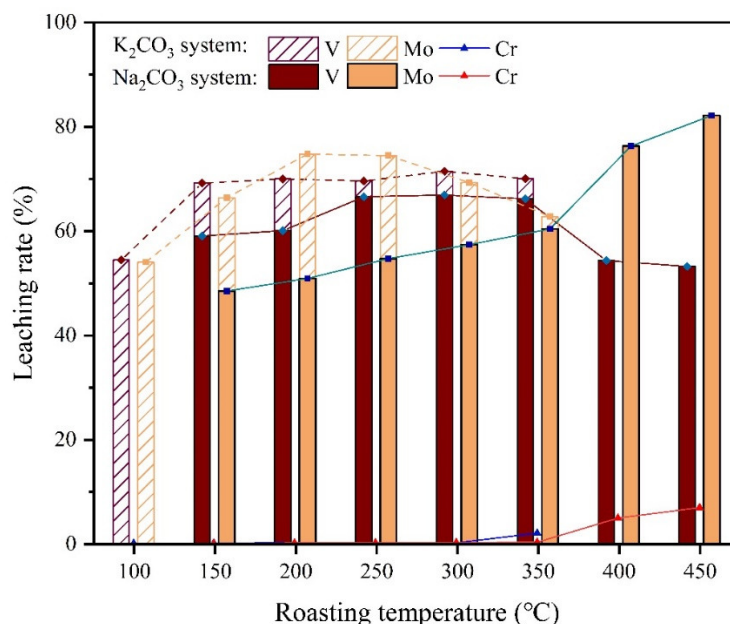


**Figure 3.** Effects of temperature on the leaching rates of V, Cr, and Mo.

When the temperature was below 300 °C, neither carbonate reacted with the ferrochrome spinel; when it exceeded 350 °C, the chromium in the ferrochrome spinel was converted into a soluble chromate. Meanwhile, a partial consumption of the carbonates by the ferrochrome spinel decreased the leaching rates of vanadium and molybdenum.

In the  $\text{Na}_2\text{CO}_3$  system, at 400 °C, the vanadium leaching rate decreased by 11.83% and the chromium and molybdenum leaching rates increased by 4.64% and 15.87%, respectively. This was because the ferrochrome spinel had consumed part of the carbonate, and the reaction between  $\text{Na}_2\text{CO}_3$  and  $\text{CaMoO}_4$  is endothermic. Increasing the temperature was conducive to the reaction.

The molybdenum leaching rate in the  $\text{K}_2\text{CO}_3$  system reached maximum at 200 °C. At temperatures between 200 and 350 °C, as indicated by the chromium leaching rate, the ferrochrome spinel did not react with  $\text{K}_2\text{CO}_3$  in large quantities. Thus, the decrease in the molybdenum leaching rate was attributable only to an increase in the temperature. When the experiment was conducted at 600 °C, the molybdenum leaching rate was 14.34%, indicating that  $\text{K}_2\text{CO}_3$  is not suitable for high-temperature HCVR treatment.

To study the different phase transformations in vanadium and molybdenum with temperature, the thermodynamic data of  $\text{CaV}_2\text{O}_6$ ,  $\text{CaMoO}_4$ ,  $\text{Na}_2\text{CO}_3$ , and  $\text{K}_2\text{CO}_3$  were obtained and the results are shown in Figure 4. The Gibbs free energy change ( $\Delta G$ ) of the reactions of  $\text{Na}_2\text{CO}_3$  and  $\text{K}_2\text{CO}_3$  with  $\text{CaMoO}_4$  at 200 °C were 2.6 and  $-11.6$  kJ/mol, respectively, suggesting that  $\text{K}_2\text{CO}_3$  can react spontaneously with  $\text{CaMoO}_4$  at 200 °C whereas  $\text{Na}_2\text{CO}_3$  cannot. At 200 °C, the  $\Delta G$  of the reaction between  $\text{K}_2\text{CO}_3$  and  $\text{CaMoO}_4$  was minimum, and it gradually increased with the temperature, which explains why the molybdenum leaching rate decreased when the temperature exceeded 200 °C. The  $\Delta G$  of the reactions of  $\text{K}_2\text{CO}_3$  and  $\text{Na}_2\text{CO}_3$  with  $\text{CaV}_2\text{O}_6$  were  $-26.9$  and  $-43.2$  kJ/mol, respectively, which were significantly less than 0, indicating spontaneous reactions.

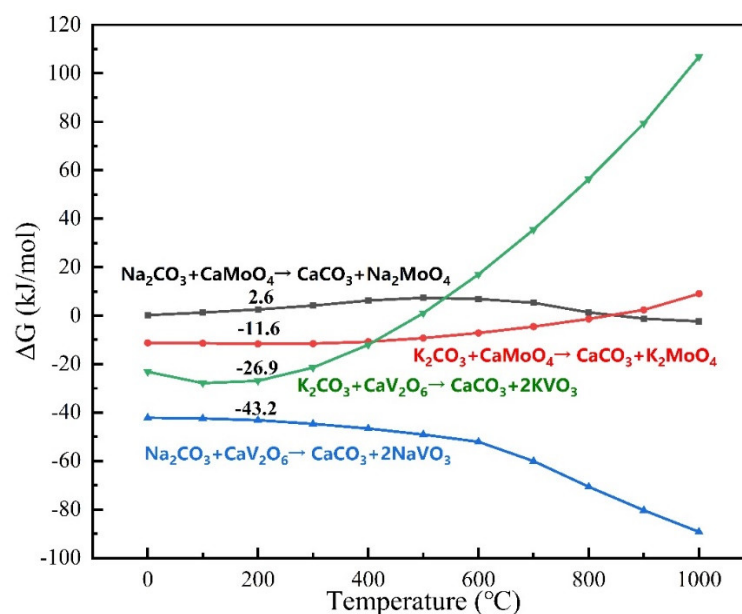


**Figure 4.**  $\Delta G$ – $T$  plots of the reactions of  $\text{K}_2\text{CO}_3$  and  $\text{Na}_2\text{CO}_3$  with  $\text{CaV}_2\text{O}_6$  and  $\text{CaMoO}_4$ .

To elucidate the phase transition during the reaction, the CHCVR was analyzed at 200 °C via XRD. Figure 5 shows the results. The diffraction peaks of  $\text{CaV}_2\text{O}_6$  and  $\text{CaMoO}_4$  were absent in the XRD patterns of the HCVR carbonation samples when  $\text{K}_2\text{CO}_3$  was used as the reagent (Figure 5b). The diffraction peaks of  $\text{CaV}_2\text{O}_6$  were absent, while those of  $\text{CaMoO}_4$  were still present, in the XRD patterns of the HCVR carbonation samples when  $\text{Na}_2\text{CO}_3$  was used as the reagent (Figure 5a). Thus,  $\text{K}_2\text{CO}_3$  had a better carbonation conversion effect on HCVR than  $\text{Na}_2\text{CO}_3$ .

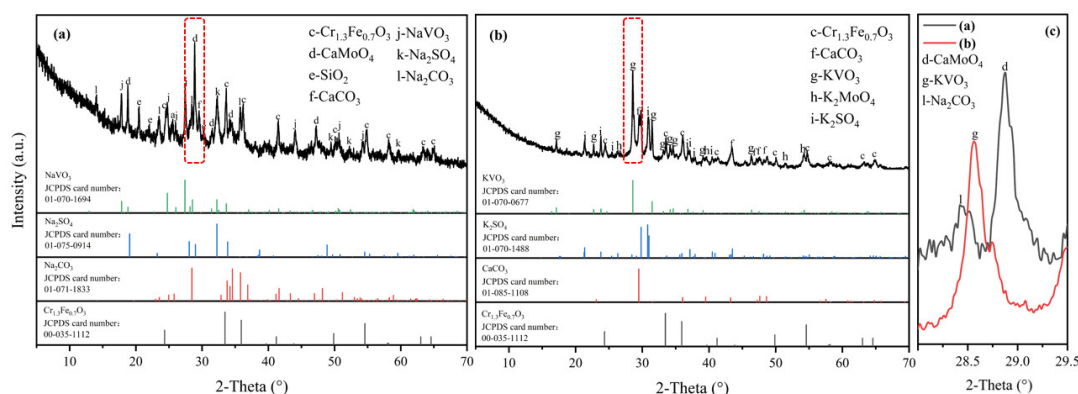


**Figure 5.** Characterization of the XRD patterns of CHCVR at 200 °C: the  $\text{Na}_2\text{CO}_3$  system (a),  $\text{K}_2\text{CO}_3$  system (b), and their magnified comparison diagram (c).

The mass and thermal changes during the carbonation conversion of HCVR were characterized via TGA, and the results are shown in Figure 6. At 80 °C, an endothermic peak was generated and the mass decreased by 1.1%, which was attributed to the evaporation of water. When the temperature exceeded 80 °C, the amount of heat generated appeared to increase rapidly, which was ascribed to the superposition of the generated exothermic peaks of  $\text{KVO}_3$  and  $\text{K}_2\text{MoO}_4$  and the endothermic peak of water evaporation. At temperatures between 100 and 350 °C,  $\text{KVO}_3$  and  $\text{K}_2\text{MoO}_4$  were continuously formed, resulting in continuous exothermic reactions. As neither reaction involved the production of gases, the mass did not change significantly. When the temperature exceeded 350 °C,  $\text{K}_2\text{CO}_3$  began to react with the chromite spinel in the HCVR to produce  $\text{CO}_2$ , resulting in a decrease in mass. At 770 °C, the amount of heat generated began to decrease rapidly, which was attributed to the decomposition of  $\text{K}_2\text{CO}_3$ .

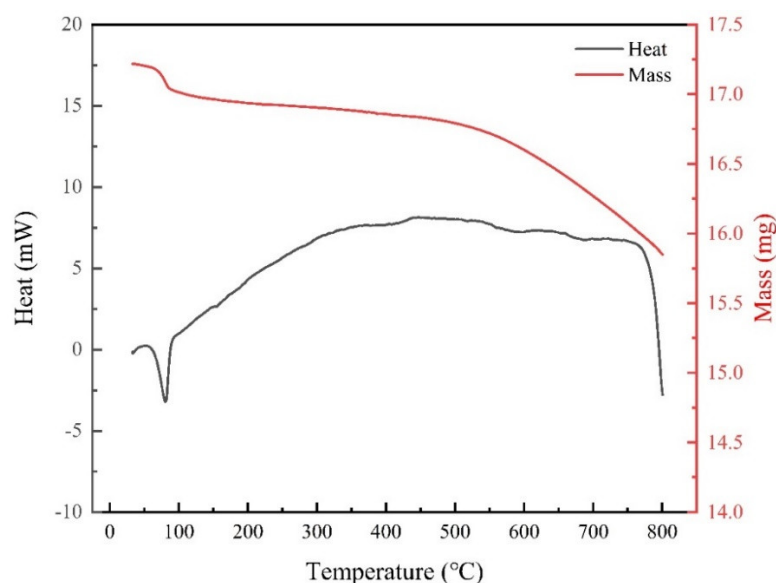


**Figure 6.** TGA characterization of HCVR during roasting with  $\text{K}_2\text{CO}_3$ .

### 3.1.2. Effect of Dosage and Time

To determine the best carbonate dosage, single-factor experiments were conducted for the carbonate amount. As indicated by Figure 3,  $\text{Na}_2\text{CO}_3$  was suitable for high-temperature reactions, whereas  $\text{K}_2\text{CO}_3$  was suitable for low-temperature reactions. Therefore, the temperatures of the two systems were set at 600 and 200 °C, respectively, while other conditions remained unchanged. Figure 7 shows the results.

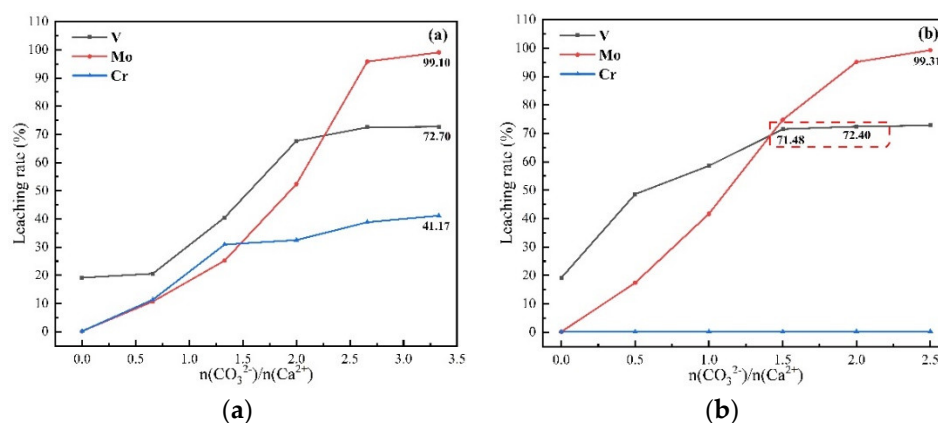
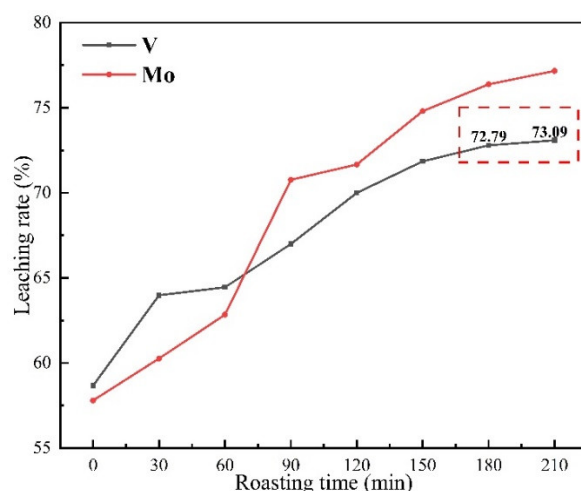


**Figure 7.** Effects of  $n(\text{CO}_3^{2-})/n(\text{Ca}^{2+})$  on the leaching rates of V, Cr, and Mo. (a)  $\text{Na}_2\text{CO}_3$  system (600 °C); (b)  $\text{K}_2\text{CO}_3$  system (200 °C).

Figure 7a shows that, at 600 °C, the leaching rates of vanadium, molybdenum and chromium increased with the  $\text{Na}_2\text{CO}_3$  dosage. With an excess of the carbonate,  $\text{CaMoO}_4$  was almost completely transformed. At insufficient dosages of the carbonate, the leaching rates of vanadium and molybdenum were low, owing to the consumption of the carbonate by the ferrochrome spinel.

Figure 7 shows that, for the same amount of the carbonate,  $\text{K}_2\text{CO}_3$  always afforded higher leaching rates of vanadium and molybdenum via the conversion of HCVR than  $\text{Na}_2\text{CO}_3$ . In the  $\text{K}_2\text{CO}_3$  system, for an  $n(\text{CO}_3^{2-})/n(\text{Ca}^{2+})$  ratio of 1.5, the vanadium leaching rate increased slightly (Figure 7b). For cost reasons,  $n(\text{CO}_3^{2-})/n(\text{Ca}^{2+}) = 1.5$  was selected as the best dosage of  $\text{K}_2\text{CO}_3$ . In general, both  $\text{Na}_2\text{CO}_3$  and  $\text{K}_2\text{CO}_3$  can effectively extract vanadium and molybdenum from HCVR; however,  $\text{K}_2\text{CO}_3$  can be used to treat HCVR at lower temperatures and dosages.

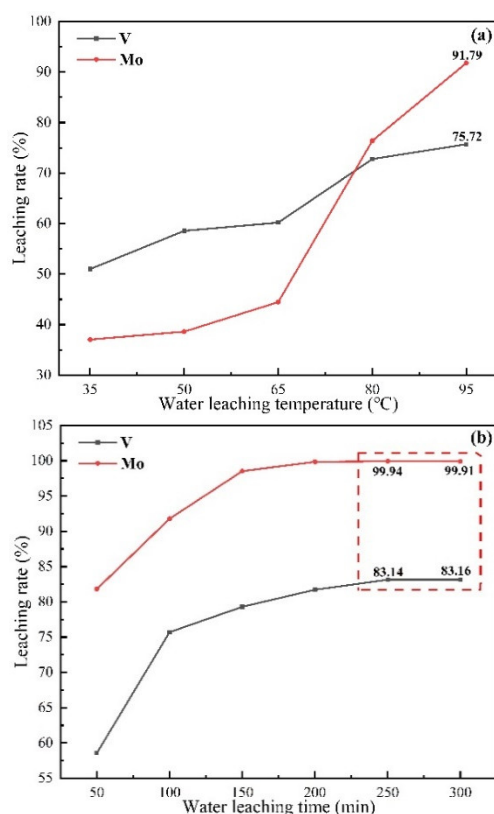
In addition, to obtain the best carbonation time parameters, a single-factor experiment was conducted for the carbonation time. The experimental conditions were as follows: temperature, 200 °C;  $n(\text{CO}_3^{2-})/n(\text{Ca}^{2+})$ , 1.5; leaching temperature, 80 °C; and leaching time, 100 min. Figure 8 shows the results. The leaching rates of vanadium and molybdenum increased continuously with the carbonation time. At a carbonation time of 180 min, the leaching rate of vanadium increased slightly. For the lowest process time, 180 min was selected as the optimal carbonation time.



**Figure 8.** Effects of  $\text{K}_2\text{CO}_3$  carbonation time on the leaching rates of V and Mo.

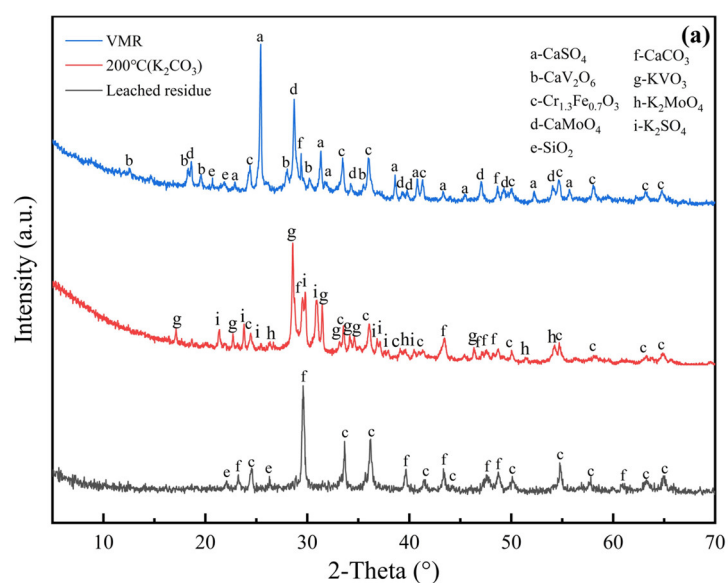
### 3.1.3. Effect of Leaching Temperature and Time

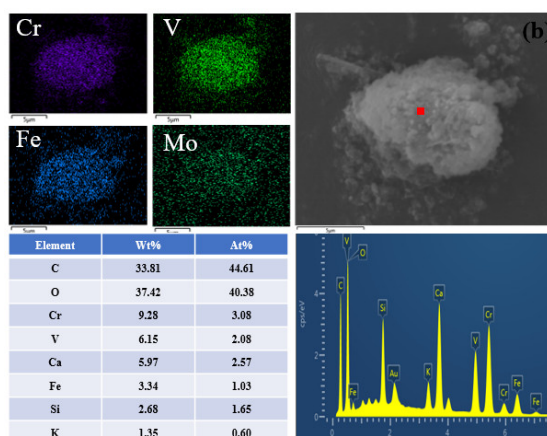
To determine the optimal leaching temperature and time, single-factor experiments were conducted for leaching temperature under the previously determined optimal reaction conditions, and single-factor experiments for leaching time were conducted at the best leaching temperature. Figure 9 shows the results. Figure 9a indicates that the leaching rates of vanadium and molybdenum gradually increased with the water leaching temperature, because a higher water temperature accelerated the dissolution rate. At a water leaching temperature of 95 °C, the leaching rates of vanadium and molybdenum were 75.72% and 91.79%, respectively; therefore, 95 °C was selected as the optimal leaching temperature for subsequent experiments. Figure 9b indicates that the leaching rates of vanadium and molybdenum gradually increased with the leaching time. A leaching time of 250 min afforded the highest leaching rates of vanadium and molybdenum, 83.14% and 99.94%, respectively, and a low leaching rate of chromium, 0.33%. Therefore, 250 min was selected as the optimal leaching time.



**Figure 9.** Effects of the water leaching temperature (a) and leaching time (b) on the leaching behaviors of V and Mo.

XRD and SEM-EDS analyses were conducted on the tailings, and the results are shown in Figure 10. Figure 10a shows that the peak of ferrochrome spinel remained unchanged, while a prominent characteristic peak of calcium carbonate appeared and the characteristic peaks of  $\text{CaV}_2\text{O}_6$  and  $\text{CaMoO}_4$  in the leaching slag almost disappeared, indicating successful carbonation. Thus,  $\text{CaV}_2\text{O}_6$  and  $\text{CaMoO}_4$  in the raw material had been completely dissolved in the solution.





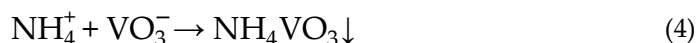
**Figure 10.** Phase-change diagram of HCVR during the entire process (a) and SEM-EDS characterization of the tailings (b).

Figure 10b shows that vanadium, chromium, and iron had obvious interactions in the tailings particles, which is consistent with the properties of ferrochrome spinel in the raw material. Ferrochrome spinel had not been consumed, and it remained in the leaching slag, while part of the vanadium still existed in the chromite spinel via isomorphism. Therefore, the vanadium leaching rate could not be further improved. The distribution of molybdenum had no correlation with these particles. Molybdenum was not detected during elemental analysis via multiple-particle dot scanning, indicating that the molybdenum in the HCVR had leached completely into the leaching solution.

### 3.2. Recovery of Vanadium and Molybdenum from a Weakly Alkaline Solution

#### 3.2.1. Separation of Vanadium and Molybdenum and Recovery of Vanadium

When the pH of the leaching liquid was in the range 9–10, an ammonium salt was added to precipitate the vanadium in the form of ammonium metavanadate [26,27], while ammonium molybdate, which has high solubility at this pH, remained in the solution. The reaction equation of vanadium precipitation is shown in Equation (4).



Thus, vanadium and molybdenum were separated by adding  $\text{NH}_4\text{Cl}$  to the leaching liquid.

Figure 11 shows the influence of various factors on vanadium precipitation and XRD characterization of the obtained  $\text{V}_2\text{O}_5$  product. Figure 11a shows that the vanadium precipitation rate increased with the amount of ammonium chloride added. This was attributed to the promotion of the forward reaction shown in Equation (4), with an excess of ammonium ions in the solution [28,29]. When the amount of  $\text{NH}_4\text{Cl}$  was four times that of vanadium in the leaching liquid, the vanadium precipitation rate was already high, and the further addition of  $\text{NH}_4\text{Cl}$  would have only increased the cost and difficulty of wastewater treatment. Therefore,  $n(\text{NH}_4\text{Cl})/n(\text{V}) = 4$  was selected as the optimal  $\text{NH}_4\text{Cl}$  dosage parameter.

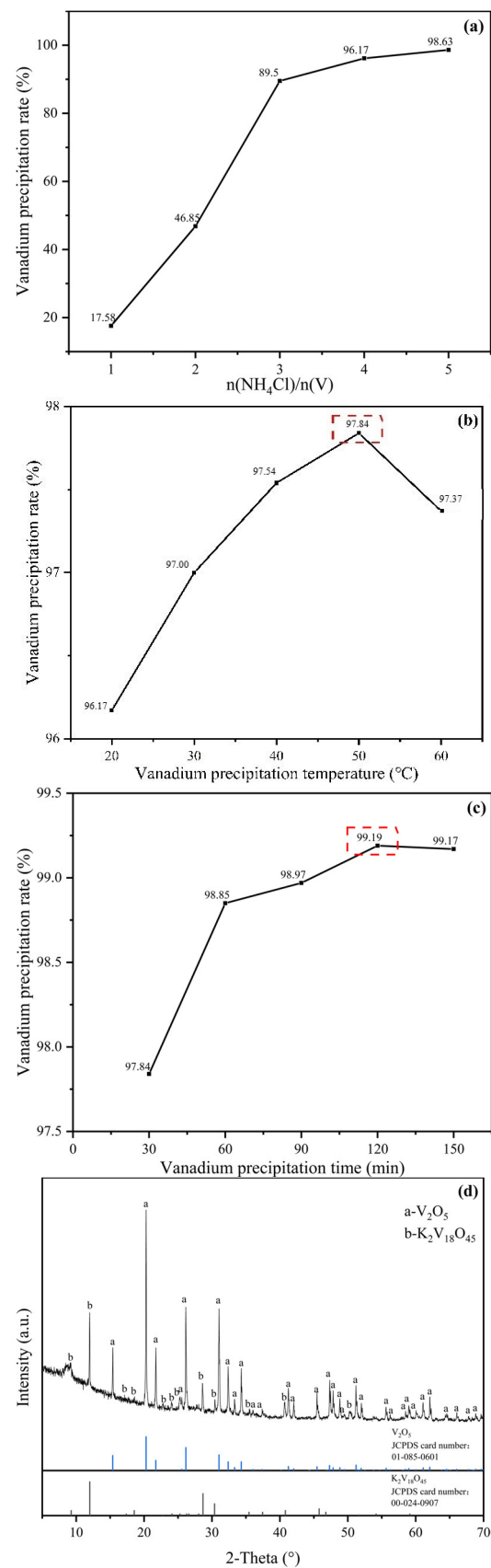


**Figure 11.** Effects of  $n(\text{NH}_4\text{Cl})/n(\text{V})$  (a), temperature (b), and time (c) on the vanadium precipitation rate. XRD patterns of the  $\text{V}_2\text{O}_5$  product (d).

Figure 11b shows the effect of temperature on the vanadium precipitation rate. At 50 °C, the vanadium precipitation rate reached a maximum, which was 97.84%. With a further increase in temperature, the vanadium precipitation rate began to decline because a higher temperature increased the solubility of ammonium metavanadate. When the water temperature exceeded 50 °C, part of the ammonium ions in the solution were lost via the evolution of ammonia. This decreased the concentration of ammonium ions in the solution, which resulted in a decrease in the vanadium precipitation rate. Therefore, the vanadium precipitation temperature was controlled to increase the rate of the reaction without generating a large amount of ammonia and reducing the concentration of ammonium ions in the solution. The optimal vanadium precipitation temperature was selected as 50 °C.

Figure 11c shows the effect of vanadium precipitation time on the vanadium precipitation rate. At a vanadium precipitation time of 120 min, the vanadium precipitation rate reached a maximum of 99.19% and subsequently decreased, which was attributed to the dissolution of ammonium metavanadate in the solution. Therefore, 120 min was determined as the optimal vanadium precipitation time.

V<sub>2</sub>O<sub>5</sub> was prepared by roasting the vanadium precipitation product at 550 °C for 2 h. ICP analysis showed that the synthesized V<sub>2</sub>O<sub>5</sub> had a purity of 98.28%, which meets the standard of Grade 98 V<sub>2</sub>O<sub>5</sub> product in YB/T 5304-2011 [30]. Table 2 shows the chemical compositions of the standard and V<sub>2</sub>O<sub>5</sub> product. Figure 11d shows the XRD patterns of the V<sub>2</sub>O<sub>5</sub> product.

**Table 2.** Chemical compositions of the standard and the V<sub>2</sub>O<sub>5</sub> product (wt.%).

Compositions	V <sub>2</sub> O <sub>5</sub>	Si	Fe	P	S	As	Na <sub>2</sub> O + K <sub>2</sub> O
V <sub>2</sub> O <sub>5</sub> (98% standard *)	>98	0.25<	0.30<	0.05<	0.03<	0.02<	1.5<
V <sub>2</sub> O <sub>5</sub> product	98.28	0.0005	0.0373	0.0005	0.0027	0.0005	1.43

\* Standard reference YB/T 5304-2011.

A comparison of Table 2 and Figure 11d indicates that the most prominent impurity in the V<sub>2</sub>O<sub>5</sub> product was K, which was present in V<sub>2</sub>O<sub>5</sub> in the form of K<sub>2</sub>V<sub>18</sub>O<sub>45</sub>. This was attributed to a high K<sup>+</sup> content in the vanadium precipitate solution. Furthermore, co-precipitation with the ammonium vanadate precipitate was facile, and potassium vanadate was present as an impurity in the ammonium vanadate precipitate. The vanadium products were purified as follows: the concentration of potassium ions was reduced by dissolving the first-precipitated ammonium vanadate and then adding ammonium chloride for secondary vanadium precipitation to reduce the content of potassium ions in the secondary ammonium vanadate product.

Figure 12 shows the results of the SEM-EDS analysis of the V<sub>2</sub>O<sub>5</sub> products. A surface scan of the V<sub>2</sub>O<sub>5</sub> product particles revealed their association with potassium, as indicated by a part of potassium being included in the ammonium vanadate precipitate as an impurity. Further, point-scan elemental composition analysis indicated that the main impurity was potassium. However, molybdenum was not detected, which was consistent with the XRD results. Vanadium and molybdenum were separated by adding NH<sub>4</sub>Cl to precipitate vanadium directly.

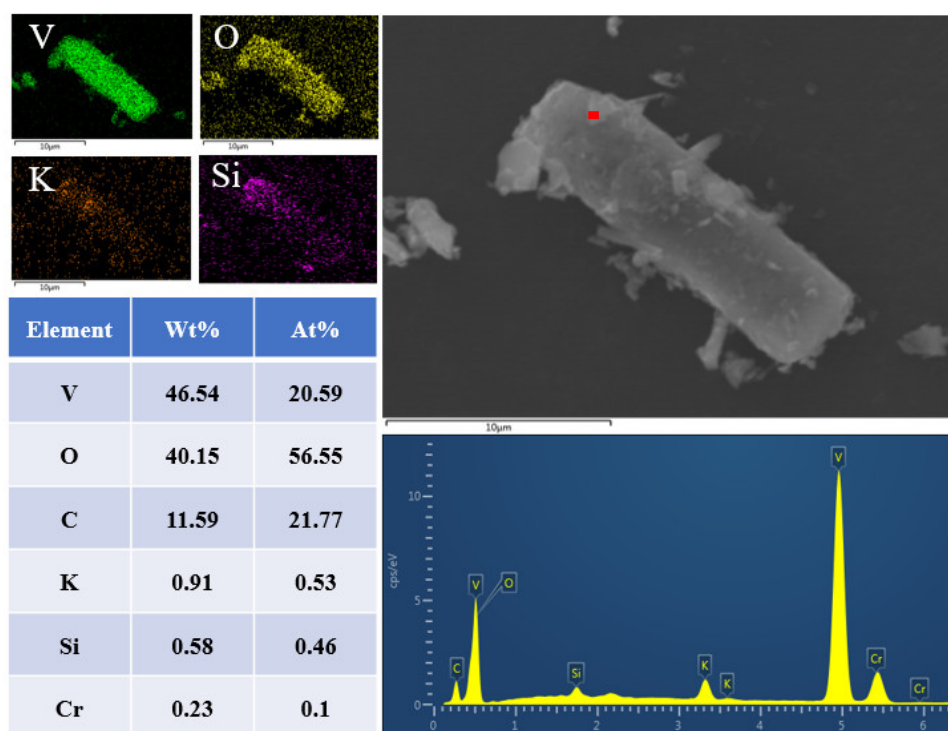


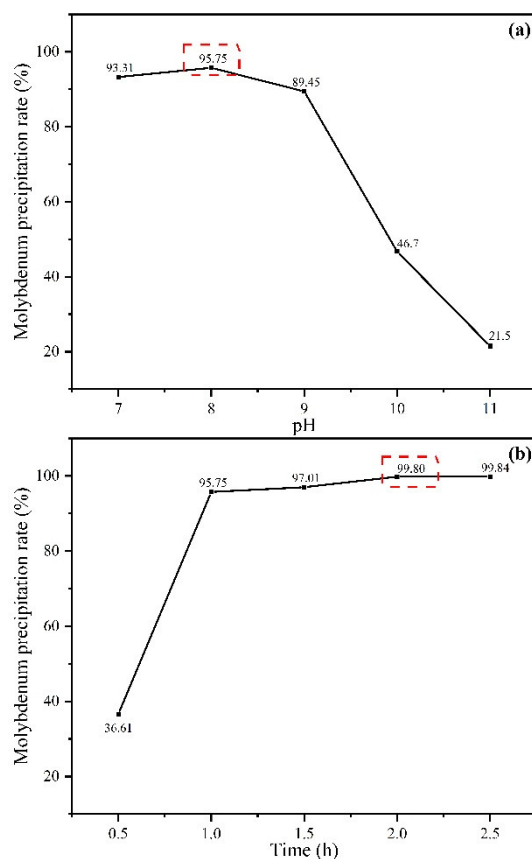
Figure 12. SEM-EDS characterization of the  $V_2O_5$  product.

### 3.2.2. Recovery of Molybdenum

The molybdenum product was recovered from the Mo-supernatant via a hydrothermal method. The effect of pH and time on the molybdenum deposition rate was studied for an  $n(Na_2S)/n(Mo)$  ratio of four and reaction temperature of 200 °C, and the results are shown in Figure 13. With a decrease in pH, the molybdenum deposition rate increased gradually, because large amounts of  $OH^-$  were produced in the process of molybdenum sulfide formation, as follows:



As shown in Equation (5), the formation of molybdenum sulfide requires the consumption of hydrogen ions. At a low initial pH, the concentration of  $H^+$  in the solution was high, resulting in a higher degree of reaction. In contrast, at a high pH, the concentration of  $H^+$  was inadequate to drive the reaction forward, resulting in a low molybdenum precipitation rate (Figure 13a). Adjusting the pH of the solution to 7 required large amounts of acid, accompanied by the release of large amounts of the highly toxic hydrogen sulfide, which also reduced the  $S^{2-}$  concentration in the solution. Therefore, the optimal pH was selected as 8. Figure 13b shows that the molybdenum precipitation rate increased with time. When the reaction time reached 2 h, 99.80% of molybdenum had been precipitated as molybdenum sulfide. Therefore, the optimal hydrothermal process time was selected as 2 h.



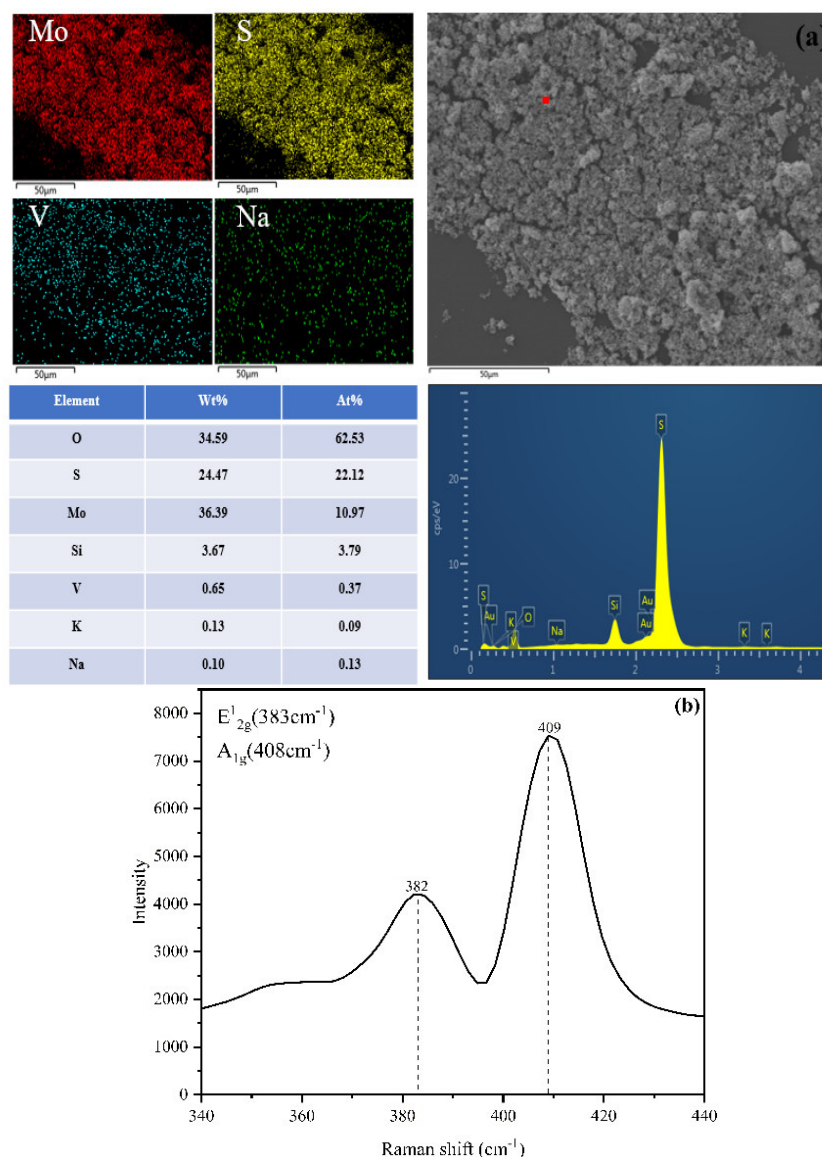
**Figure 13.** Effects of pH (a) and time (b) on the molybdenum precipitation rate.

Figure 14a,b show the SEM-EDS and Raman spectroscopy results, respectively, of the molybdenum sulfide products. Figure 14a shows significant agglomeration in the molybdenum sulfide products. A surface scan of the molybdenum sulfide particles revealed association between molybdenum and sulfur, whereas other impurity elements had low associations and contents. Point-scanning elemental analysis indicated that the atomic ratio of sulfur and molybdenum in the particles was 2.016, which is close to that of molybdenum disulfide. Table 3 shows the chemical compositions of the standard and MoS<sub>2</sub> product. The MoS<sub>2</sub> mass fraction in the synthesized MoS<sub>2</sub> product was 98.65%, which meets the standard of Grade 98 MoS<sub>2</sub> products in GB/T 23271-2009 [31].

**Table 3.** Chemical compositions of the standard and MoS<sub>2</sub> product (wt.%).

Compositions	MoS <sub>2</sub>	Total Insolubles	Fe	Pb	MoO <sub>3</sub>	SiO <sub>2</sub>	H <sub>2</sub> O
MoS <sub>2</sub> (98% standard *)	>98	0.65<	0.30<	0.02<	0.20<	0.20<	0.20<
MoS <sub>2</sub> product	98.65	0.31	0.034	0.001	0.03	0.069	0.18

\* Standard reference GB/T 23271-2009.



**Figure 14.** SEM–EDS (a) and Raman spectroscopy (b) characterization of the MoS<sub>2</sub> product.

MoS<sub>2</sub> was composed of a molybdenum disulfide molecular layer, which comprised two sulfur atomic layers surrounding a molybdenum atomic layer, wherein the atoms were combined via covalent bonds. The molybdenum disulfide molecular layers interacted via van der Waals forces and vibrated in the A<sub>1g</sub> vibration mode, whereas the molybdenum sulfide layers vibrated in the E<sub>2g</sub> vibration mode. The Raman spectra of the molybdenum sulfide products under a 532-nanometer laser revealed sharp vibration peaks at 383 and 408 cm<sup>-1</sup>, which conformed to the A<sub>1g</sub> and E<sub>2g</sub> vibration of molybdenum disulfide [32,33]. This confirmed that the synthesized molybdenum sulfide product was MoS<sub>2</sub>.

### 3.2.3. Quantity–Quality Flowsheet of the Recovered V and Mo

Figure 15 shows the quantity–quality flowsheet of the whole process. The maximum final recovery rates of vanadium and molybdenum were 82.47% and 98.88%, respectively. The unrecycled vanadium existed in the tailings mainly in the form of spinel. Molybdenum in the HCVR had been recovered. The main valuable metals in the tailings were vanadium and chromium. The tailings were returned to the main vanadium extraction process, employing vanadium slag to extract Cr and V. Table 4 shows the process parameters of treating HCVR with a different roasting reagent. The K<sub>2</sub>CO<sub>3</sub> roasting process has a high recovery rate of molybdenum and the roasting temperature decreases from 850 °C to 200 °C

compared with the  $\text{Na}_2\text{CO}_3$  roasting process. Due to the low roasting temperature, the simultaneous leaching of vanadium and chromium was avoided. Vanadium precipitation pretreatment is not required, and the obtained vanadium product has high purity.

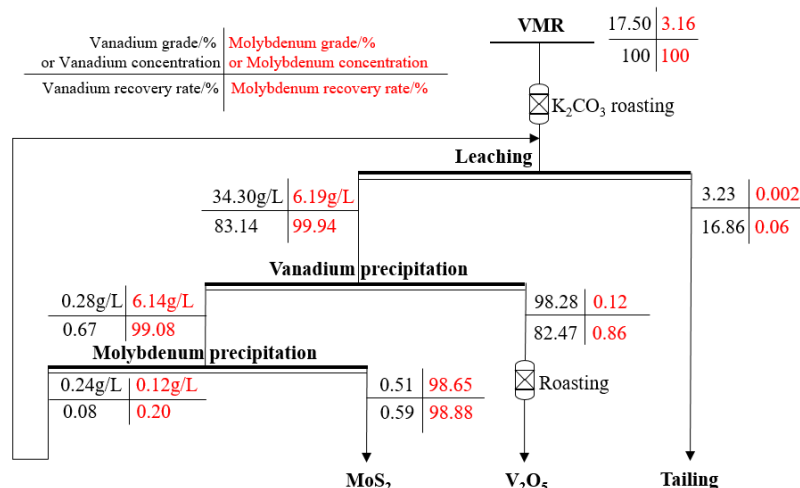


Figure 15. Quantity–quality flowsheet of the recovered vanadium and molybdenum.

Table 4. Process parameters of treating HCVR with different roasting reagent.

Reagents	Roasting Temperature	Recovery	V Precipitation Pretreatment	Production Purity	Ref.
$\text{K}_2\text{CO}_3$	200 °C	V:82.47% Mo:98.88%	-	V <sub>2</sub> O <sub>5</sub> :98.28% MoS <sub>2</sub> :98.65%	This work
$\text{Na}_2\text{CO}_3$	850 °C	V:89% Cr:95%	Adjust pH	V <sub>2</sub> O <sub>5</sub> :91.49% Cr <sub>2</sub> O <sub>3</sub> :89.89%	[17]

#### 4. Conclusions

This study proposes high-efficiency stepped separation and recoveries of vanadium and molybdenum via the low-temperature carbonation conversion of HCVR. The optimal process parameters are as follows. For carbonation conversion: 200 °C, 3 h, and molar ratio of  $\text{K}_2\text{CO}_3$  and  $\text{Ca}^{2+}$  in HCVR ( $n(\text{K}_2\text{CO}_3)/n(\text{Ca}^{2+}) = 1.5$ ); for leaching: 95 °C and 250 min; for vanadium precipitation: molar ratio of  $\text{NH}_4\text{Cl}$  and V in the leaching liquid ( $n(\text{NH}_4\text{Cl})/n(\text{V}) = 4$ , 50 °C, and 2 h; for molybdenum precipitation: molar ratio of  $\text{Na}_2\text{S}$  and Mo in the Mo-supernatant ( $n(\text{Na}_2\text{S})/n(\text{Mo}) = 4$ , 200 °C, and 2 h. Using the aforementioned conditions, 83.14% of vanadium and 99.94% of molybdenum are leached; 99.19% of vanadium is precipitated and converted into  $\text{V}_2\text{O}_5$ , with a purity of 98.28%; and 99.80% of molybdenum is precipitated as  $\text{MoS}_2$ , with a purity of 98.65%. The recovery rates of vanadium and molybdenum are 82.47% and 98.88%, respectively.

Compared with the  $\text{Na}_2\text{CO}_3$ -assisted-roasting–water-leaching method, which operates at 800 °C, the  $\text{K}_2\text{CO}_3$ -assisted-roasting–water-leaching method operates at a lower reaction temperature of 200 °C and has a better extraction effect on molybdenum for the same amount of carbonate used, owing to a more negative  $\Delta G$  of the reaction between  $\text{K}_2\text{CO}_3$  and  $\text{CaMoO}_4$  at a low temperature. Moreover, owing to the lower roasting temperature, the chromite spinel does not react with  $\text{K}_2\text{CO}_3$ ; only 0.33% of chromium is leached, and vanadium and chromium are effectively separated. Thus,  $\text{K}_2\text{CO}_3$  might be a more effective alternative to  $\text{Na}_2\text{CO}_3$  for the separation and recovery of V and Mo from HCVR and, hence, enable its more efficient utilization.

**Author Contributions:** J.Z.: Conceptualization, Methodology, Investigation, Data Curation, Writing—Original Draft, Writing—Review and Editing. N.X.: Validation, Writing—Review and Editing, Supervision, Funding acquisition. Y.Z.: Resources, Validation, Writing—Review and Editing, Supervision, Funding acquisition. Q.Z.: Validation, Writing—Review and Editing, Supervision, Project administration. All authors have read and agreed to the published version of the manuscript.

**Funding:** This study was financially supported by the National Key R&D Program of China (2018YFC1900505), the National Natural Science Foundation of China (No.52174260), and the Outstanding Young and Middle-aged Science and Technology Innovation Team Project of Hubei Province (T201802).

**Data Availability Statement:** The data that support the findings of this study are available from the corresponding author, [Xue, N.], upon reasonable request.

**Conflicts of Interest:** We have no known competing financial interests or personal relationships that could have appeared to influence the work reported in this paper.

## References

1. Zhang, Y.-M.; Bao, S.-X.; Liu, T.; Chen, T.-J.; Huang, J. The technology of extracting vanadium from stone coal in China: History, current status and future prospects. *Hydrometallurgy* **2011**, *109*, 116–124. <https://doi.org/10.1016/j.hydromet.2011.06.002>.
2. Xue, N.-N.; Zhang, Y.-M.; Liu, T.; Huang, J.; Zheng, Q.-S. Effects of hydration and hardening of calcium sulfate on muscovite dissolution during pressure acid leaching of black shale. *J. Clean. Prod.* **2017**, *149*, 989–998. <https://doi.org/10.1016/j.jclepro.2017.02.152>.
3. Zhang, G.; Zhang, Y.; Bao, S.; Yuan, Y.; Jian, X.; Li, R. Selective vanadium extraction from vanadium bearing ferro-phosphorus via roasting and pressure hydrogen reduction. *Sep. Purif. Technol.* **2019**, *220*, 293–299. <https://doi.org/10.1016/j.seppur.2019.03.076>.
4. Wen, J.; Jiang, T.; Wang, J.; Gao, H.; Lu, L. An efficient utilization of high chromium vanadium slag: Extraction of vanadium based on manganese carbonate roasting and detoxification processing of chromium-containing tailings. *J. Hazard. Mater.* **2019**, *378*, 120733. <https://doi.org/10.1016/j.jhazmat.2019.06.010>.
5. Liu, H.; Zhang, Y.-M.; Huang, J.; Liu, T. Vanadium(IV) solvent extraction enhancement in high acidity using di-(2-ethylhexyl)phosphoric acid with [Cl<sup>-</sup>] present: An experimental and theoretical study. *Front. Chem. Sci. Eng.* **2022**, 1–12. <https://doi.org/10.1007/s11705-022-2185-8>.
6. Liu, H.; Zhang, Y.-M.; Huang, J.; Liu, T.; Wang, Y.-P. Coordination extraction for separating vanadium and impurities from black shale HCl leachate at low pH using D2EHPA and EHEHPA mixture. *Sep. Purif. Technol.* **2022**, *302*, 122088. <https://doi.org/10.1016/j.seppur.2022.122088>.
7. Henckens, M.; Driessen, P.; Worrell, E. Molybdenum resources: Their depletion and safeguarding for future generations. *Resour. Conserv. Recycl.* **2018**, *134*, 61–69. <https://doi.org/10.1016/j.resconrec.2018.03.002>.
8. Baritto, M.; Oni, A.; Kumar, A. The development of a techno-economic model for the assessment of vanadium recovery from bitumen upgrading spent catalyst. *J. Clean. Prod.* **2022**, *363*, 132376. <https://doi.org/10.1016/j.jclepro.2022.132376>.
9. Chen, B.; Wang, M.; Huang, S.; Ge, Q.; Wang, X.; Sun, B. Extraction of vanadium from V-Cr bearing reduced residue by selective oxidation combined with alkaline leaching. *Can. Met. Q.* **2018**, *57*, 434–438. <https://doi.org/10.1080/00084433.2018.1491161>.
10. Chen, B.; Huang, S.; Liu, B.; Ge, Q.; Wang, M.; Wang, X. Separation and recovery of vanadium and chromium from acidic leach solution of V-Cr-bearing reducing slag. *J. Environ. Chem. Eng.* **2017**, *5*, 4702–4706. <https://doi.org/10.1016/j.jece.2017.09.001>.
11. Wen, J.; Jiang, T.; Zhou, W.; Gao, H.; Xue, X. A cleaner and efficient process for extraction of vanadium from high chromium vanadium slag: Leaching in (NH<sub>4</sub>)<sub>2</sub>SO<sub>4</sub>-H<sub>2</sub>SO<sub>4</sub> synergistic system and NH<sub>4</sub><sup>+</sup> recycle. *Sep. Purif. Technol.* **2019**, *216*, 126–135. <https://doi.org/10.1016/j.seppur.2019.01.078>.
12. Teng, A.; Xue, X. A novel roasting process to extract vanadium and chromium from high chromium vanadium slag using a NaOH-NaNO<sub>3</sub> binary system. *J. Hazard. Mater.* **2019**, *379*, 120805–120814. <https://doi.org/10.1016/j.jhazmat.2019.120805>.
13. Wen, J.; Jiang, T.; Sun, H.; Yu, T.; Li, M.; Peng, Y. Investigation on separation principle of vanadium and chromium among Fe<sub>2</sub>VO<sub>4</sub>-CaO-FeCr<sub>2</sub>O<sub>4</sub> system: Simplify and simulate calcification roasting process of vanadium-chromium slag. *J. Ind. Eng. Chem.* **2022**, *115*, 378–389. <https://doi.org/10.1016/j.jiec.2022.08.022>.
14. Wang, M.; Chen, B.; Huang, S.; Wang, X.; Liu, B.; Ge, Q.; Xie, S. A novel technology for vanadium and chromium recovery from V-Cr-bearing reducing slag. *Hydrometallurgy* **2017**, *171*, 116–122. <https://doi.org/10.1016/j.hydromet.2017.05.007>.
15. Yang, Y.; Ye, Y.; Zhang, C.; Yang, H. Study on extracting technology of vanadium and chromium by acid leaching. *Inorg. Chem. Ind.* **2014**, *46*, 59–61.
16. Yin, R.; Chen, L.; Qin, Z.; Xiao, H.; Weng, D.; Liang, B.; Wang, Z.; Luo, D. A novel complexation method for separation and recovery of low valence vanadium, iron and chromium from sulfuric acid solution. *J. Clean. Prod.* **2022**, *373*, 133640. <https://doi.org/10.1016/j.jclepro.2022.133640>.
17. Wen, J.; Jiang, T.; Xu, Y.; Cao, J.; Xue, X. Efficient extraction and separation of vanadium and chromium in high chromium vanadium slag by sodium salt roasting-(NH<sub>4</sub>)<sub>2</sub>SO<sub>4</sub> leaching. *J. Ind. Eng. Chem.* **2018**, *71*, 327–335. <https://doi.org/10.1016/j.jiec.2018.11.043>.

18. Fan, H.; Duan, H.; He, W.; Chen, D.; Liu, T.; Long, M.; Xu, P. Sequential extraction of vanadium and chromium from chromium-bearing vanadium slag through two-stage soda roasting–water leaching. *Met. Res. Technol.* **2018**, *115*, 607. <https://doi.org/10.1051/metal/2018093>.
19. Cheng, J.; Li, H.-Y.; Chen, X.-M.; Hai, D.; Diao, J.; Xie, B. Eco-friendly chromium recovery from hazardous chromium-containing vanadium extraction tailings via low-dosage roasting. *Process. Saf. Environ. Prot.* **2022**, *164*, 818–826. <https://doi.org/10.1016/j.psep.2022.06.065>.
20. Wen, J.; Jiang, T.; Gao, H.; Zhou, W.; Xu, Y.; Zheng, X.; Liu, Y.; Xue, X. An efficient utilization of chromium-containing vanadium tailings: Extraction of chromium by soda roasting–water leaching and preparation of chromium oxide. *J. Environ. Manag.* **2019**, *244*, 119–126. <https://doi.org/10.1016/j.jenvman.2019.05.037>.
21. Zhang, X.; Meng, F.; Zhu, Z.; Chen, D.; Zhao, H.; Liu, Y.; Zhen, Y.; Qi, T.; Zheng, S.; Wang, M.; et al. A novel process to prepare high-purity vanadyl sulfate electrolyte from leach liquor of sodium-roasted vanadium slag. *Hydrometallurgy* **2021**, *208*, 105805. <https://doi.org/10.1016/j.hydromet.2021.105805>.
22. Ying, Z.; Song, Y.; Zhu, K.; Wu, G.; Ju, Y.; Wei, Q.; Ren, X. A cleaner and sustainable method to recover vanadium and chromium from the leaching solution based on solvent extraction. *J. Environ. Chem. Eng.* **2022**, *10*, 107384. <https://doi.org/10.1016/j.jece.2022.107384>.
23. Liu, C.; Ji, H.; Liu, J.; Liu, P.; Zeng, G.; Luo, X.; Guan, Q.; Mi, X.; Li, Y.; Zhang, J.; et al. An emission-free controlled potassium pyrosulfate roasting-assisted leaching process for selective lithium recycling from spent Li-ion batteries. *Waste Manag.* **2022**, *153*, 52–60. <https://doi.org/10.1016/j.wasman.2022.08.021>.
24. Ye, L.; Ouyang, Z.; Chen, Y.; Liu, S. Recovery of rhenium from tungsten-rhenium wire by alkali fusion in KOH-K<sub>2</sub>CO<sub>3</sub> binary molten salt. *Int. J. Refract. Met. Hard Mater.* **2019**, *87*, 105148. <https://doi.org/10.1016/j.ijrmhm.2019.105148>.
25. Li, H.-Y.; Wang, C.; Lin, M.; Guo, Y.; Xie, B. Green one-step roasting method for efficient extraction of vanadium and chromium from vanadium-chromium slag. *Powder Technol.* **2020**, *360*, 503–508. <https://doi.org/10.1016/j.powtec.2019.10.074>.
26. Xiong, P.; Zhang, Y.; Bao, S.; Huang, J. Precipitation of vanadium using ammonium salt in alkaline and acidic media and the effect of sodium and phosphorus. *Hydrometallurgy* **2018**, *180*, 113–120. <https://doi.org/10.1016/j.hydromet.2018.07.014>.
27. Navarro, R.; Guzmán-Pantoja, J.; Saucedo, I.; Revilla, J.; Guibal, E. Vanadium recovery from oil fly ash by leaching, precipitation and solvent extraction processes. *Waste Manag.* **2007**, *27*, 425–438. <https://doi.org/10.1016/j.wasman.2006.02.002>.
28. Chen, B.; Bao, S.; Zhang, Y.; Ren, L. A novel and sustainable technique to precipitate vanadium from vanadium-rich solutions via efficient ultrasound irradiation. *J. Clean. Prod.* **2022**, *339*, 130755. <https://doi.org/10.1016/j.jclepro.2022.130755>.
29. Du, G.; Sun, Z.; Xian, Y.; Jing, H.; Chen, H.; Yin, D. The nucleation kinetics of ammonium metavanadate precipitated by ammonium chloride. *J. Cryst. Growth* **2016**, *441*, 117–123. <https://doi.org/10.1016/j.jcrysgro.2016.02.016>.
30. YB/T 5304-2011; Vanadium Pentoxide. Chinese Standard: Beijing, China 2011.
31. GB/T 23271-2009; Molybdenum Disulfide. Chinese Standard: Beijing, China, 2009.
32. Li, Y.; Nakamura, R. Structural change of molybdenum sulfide facilitates the electrocatalytic hydrogen evolution reaction at neutral pH as revealed by in situ Raman spectroscopy. *Chin. J. Catal.* **2018**, *39*, 401–406. [https://doi.org/10.1016/S1872-2067\(17\)62945-0](https://doi.org/10.1016/S1872-2067(17)62945-0).
33. Kaur, N.; Mir, R.A.; Pandey, O. A novel study on soft ferromagnetic nature of nano molybdenum sulphide (MoS<sub>2</sub>). *Phys. B Condens. Matter* **2019**, *574*, 411684. <https://doi.org/10.1016/j.physb.2019.411684>.

**Disclaimer/Publisher’s Note:** The statements, opinions and data contained in all publications are solely those of the individual author(s) and contributor(s) and not of MDPI and/or the editor(s). MDPI and/or the editor(s) disclaim responsibility for any injury to people or property resulting from any ideas, methods, instructions or products referred to in the content.